Zeitschrift: Eclogae Geologicae Helvetiae

Band: 73 (1980)

Heft: 2: Symposium alpine geotraverses with special emphasis on the Basel-Chiasso profile : Lausanne, 4-5 October 1979

Artikel: Comparison of focal mechanisms of earthquakes and faulting in the Helvetic zone of the Central Valais, Swiss Alps

Autor: Pavoni, Nazario

DOI: https://doi.org/10.5169/seals-164973

Eclogae geol. Helv.	Vol. 73/2	Pages 551-558	6 figures in the text	Basle, July 1980

Comparison of focal mechanisms of earthquakes and faulting in the Helvetic zone of the Central Valais, Swiss Alps[1])

By NAZARIO PAVONI[2])

ABSTRACT

The technique, by which an earthquake fault-plane solution is represented, has been applied to observed displacements on faults. The procedure allows a direct comparison of geological and seismological data. Comparison of late-Alpine faulting in the Helvetic zone of the Central Valais (Fig. 5, 6) with composite fault-plane solutions of microearthquakes of the Wildhorn zone (Fig. 2, 3) reveals the close relationship between present tectonic movements and neotectonic faulting.

ZUSAMMENFASSUNG

Das in der Seismologie zur Darstellung von Herdmechanismen von Erdbeben verwendete Verfahren lässt sich in sinngemässer Übertragung auch für die Darstellung von Brüchen und Verschiebungen verwenden. Das Vorgehen wird in Abschnitt 4 kurz erläutert. Die so erhaltenen Verschiebungs-Diagramme von Brüchen ermöglichen einen direkten Vergleich geologischer und seismologischer Befunde. Ein Vergleich von Verschiebungs-Diagrammen spätalpiner Bruchstrukturen im Helvetikum des Mittelwallis (Fig. 5, 6) mit Herdlösungen von Mikroerdbeben der Wildhornzone (Fig. 2, 3) lässt sehr deutlich die enge Beziehung zwischen den heutigen tektonischen Bewegungen und den neotektonischen Verschiebungen erkennen.

1. Introduction

The Central Valais is one of the seismically most active regions of Switzerland. A rather regular continuous seismicity is documented for this region in the Annual Reports of the Swiss Seismological Service. Microearthquake surveys were conducted for several weeks in 1975, 1976 and 1977 on the northern slope of the Rhone valley between Wildstrubel and Sanetsch-Pass, using a network of five portable stations. The area investigated is part of the epicentral and aftershock area of the 1946 Valais earthquake (estimated magnitude $M_{I_o} = 5.7$).

2. Seismicity and tectonics of the Wildhorn seismic zone

Figure 1 shows the distribution of epicenters of microearthquakes recorded during the surveys in 1976 and 1977. The main seismic activity is concentrated in a

---

[1]) Contribution No. 291 of the Institute of Geophysics, ETH-Hönggerberg, CH-8093 Zürich.

[2]) Institut für Geophysik, ETH-Hönggerberg, CH-8093 Zürich.

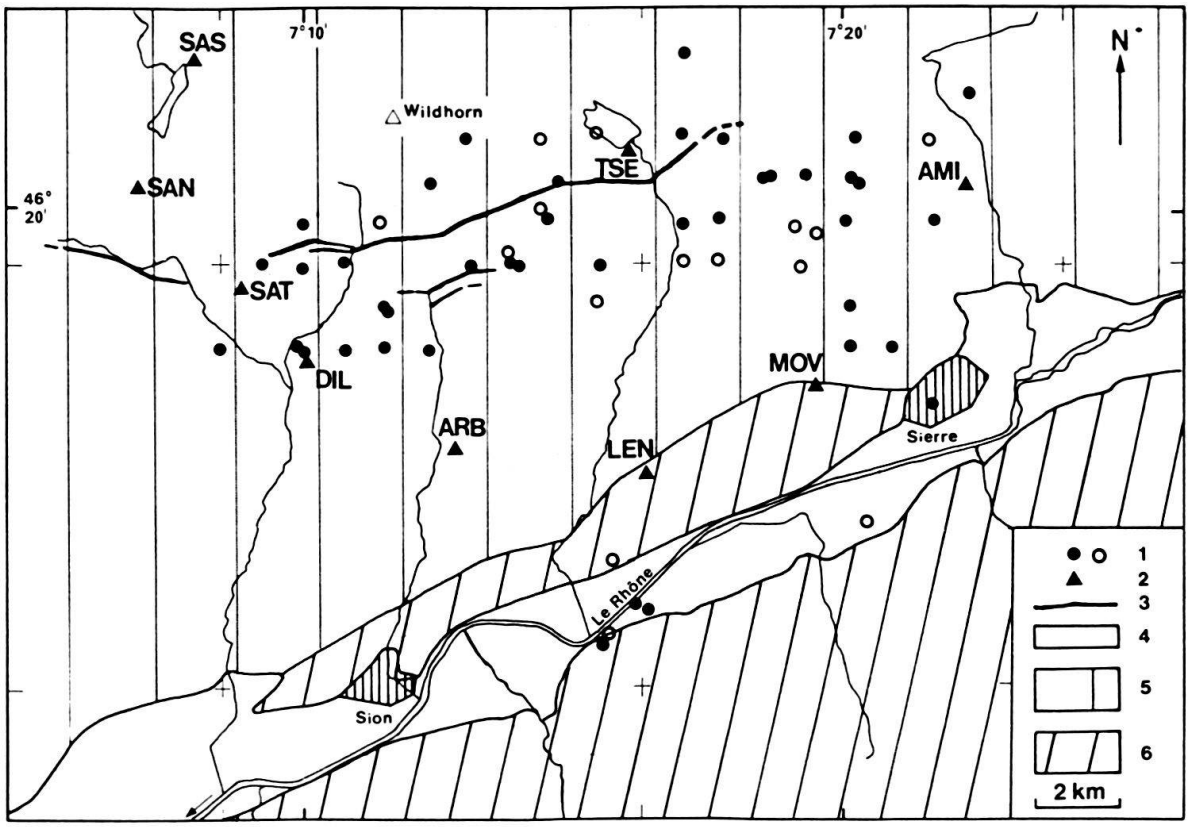

Fig. 1. Distribution of epicenters of microearthquakes during May/June 1976 and June 1977 in the Central Valais. *1* = Epicenters from 24 May to 16 June 1976 (dots) and 16-30 June 1977 (circles), *2* = temporary station, *3* = observed late-Alpine faults of the Wildhorn seismic zone (schematic), *4* = Quaternary deposits of the Rhone valley plain, *5* = Helvetic and Ultra-Helvetic nappes, *6* = Pennine nappes.

WSW-ENE trending zone, the Wildhorn seismic zone (PAVONI 1977, 1980), about 4 km wide and 20 km long, between La Fava-Sex Rouge-Zeuzier-Mont Bonvin. About 80% of the events were located in this zone. The focal depths of the microearthquakes within the Wildhorn zone range in depth from 1 to 10 km, their magnitudes M_L from $+0.2$ to $+2.5$. The accuracy of epicenter determination within the station net is about ± 1 km.

The Wildhorn zone is situated in the Helvetic zone (BADOUX et al. 1959). According to their depth the foci are situated either in the Helvetic nappes or in the sedimentary cover and the crystalline basement of the Aar massif. Of special interest is a system of WSW-ENE trending faults which can be traced in the Wildhorn zone from Le Serac in the west over Chable Court and Sex Rouge into the Vallon des Andins. It crosses the Liène valley south of Vatseret. The faults cut through the nappes structures of the Wildhorn nappe. These longitudinal faults may represent the surface expression of the W-E fault system revealed by the fault-plane solutions (Fig. 2, 3), although it was not possible to correlate any event directly with a mapped fault. During the 1946 Valais earthquake and its aftershocks several landslides were triggered along this zone, a major one at the Six des Eaux Froides, its debris covering the floor of the Vallon des Andins.

3. Fault-plane solutions from microearthquakes of the Wildhorn zone

Three composite fault-plane solutions based on microearthquakes which occurred in the central and eastern parts of the Wildhorn zone are shown in Figures 2 and 3. Circles denote dilation, full circles (dots) compression in lower hemisphere equal area projection. The compressional quadrants are hatched. The three solutions indicate a strike-slip type mechanism, with dextral strike-slip on an E–W striking, vertical or nearly vertical fault plane, and/or sinistral strike-slip on a N–S trending, steeply dipping fault plane. The corresponding *P*- and *T*-axes are nearly horizontal. The *P*-axes are oriented NW–SE, the *T*-axes NE–SW. Evidently the solutions represent the more frequent types of earthquake-generating tectonic movements in the Wildhorn zone.

The purpose of this paper is to compare the focal mechanism with the young, Alpine fault tectonics observed in the Wildhorn zone. To facilitate a comparison of

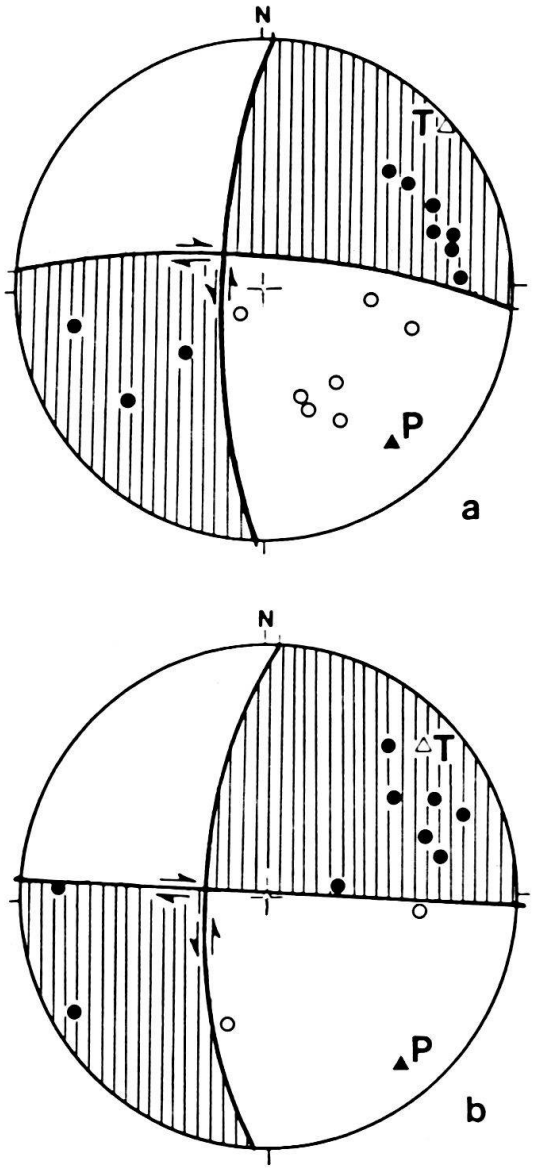

Fig. 2. Composite fault-plane solutions based on microearthquakes of the eastern (*a*) and central (*b*) Wildhorn zone, May/June 1976. Lower hemisphere equal area projection. Dots: Compression, circles: Dilatation. Hatched: Compressional quadrants. *P*: *P*-axis trend/plunge 140/21 (*a*), 141/15 (*b*). *T*: *T*-axis 50/2 (*a*), 49/15 (*b*).

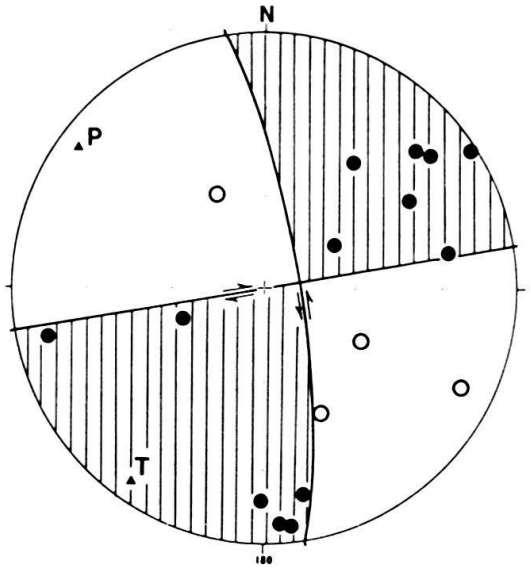

Fig. 3. Composite fault-plane solution based on microearthquakes of the eastern Wildhorn zone, June 1977. Legend see Figure 2. *P*-axis 306/9, *T*-axis 214/9.

results of these two independent types of information a method was developed to translate the observations of the geologist into the language of the seismologist.

4. Representation of faults, fault diagrams

Figure 4 shows graphically the relationship which is generally assumed to exist between the type of faulting, stress distribution and the type of fault-plane solution, and which forms the basis for the methodology used in this paper. The relationship is shown in the case of reverse faulting (*A*), normal faulting (*B*), strike-slip faulting (*C*) and oblique faulting (*D*).

In order to represent an observed fault or displacement in a manner similar to that with which the seismologist represents a fault-plane solution of an earthquake, the following procedure is proposed (all constructions on lower hemisphere projection, see Figure 5):

For a given location the pole (*Y*) of the fault plane (*S*) is determined. The slip vector $\bar{L}$ is deduced from the slickensides on the fault plane *S*. By definition $\bar{L}$ corresponds to the displacement direction of the hanging wall relative to the footwall. The intersection point (*L*) with the unit sphere is then found. An auxiliary plane *E* with pole *X* (= point *L*), normal to the fault plane *S* and normal to the slip vector $\bar{L}$, is constructed.

Fault plane *S* and auxiliary plane *E* divide the unit sphere into four quadrants. The sense of relative displacement on the fault plane *S* defines "compressional" (*C*) and "dilatation" (*D*) quadrants which are emphasized by hatching of the *C*-quadrants (Fig. 5). A second auxiliary plane *A* (trace *a*), normal to the fault plane and plane *E*, with pole *Z* (= point *B*), is determined. Points *P* and *T* are located on trace *a* at 45° distance from *L*. *P* ist situated in the *D*-quadrant, *T* in the *C*-quadrant. *P* is the intersection point of the axis of maximum shortening with the unit sphere, *T* the intersection point of the axis of maximum elongation.

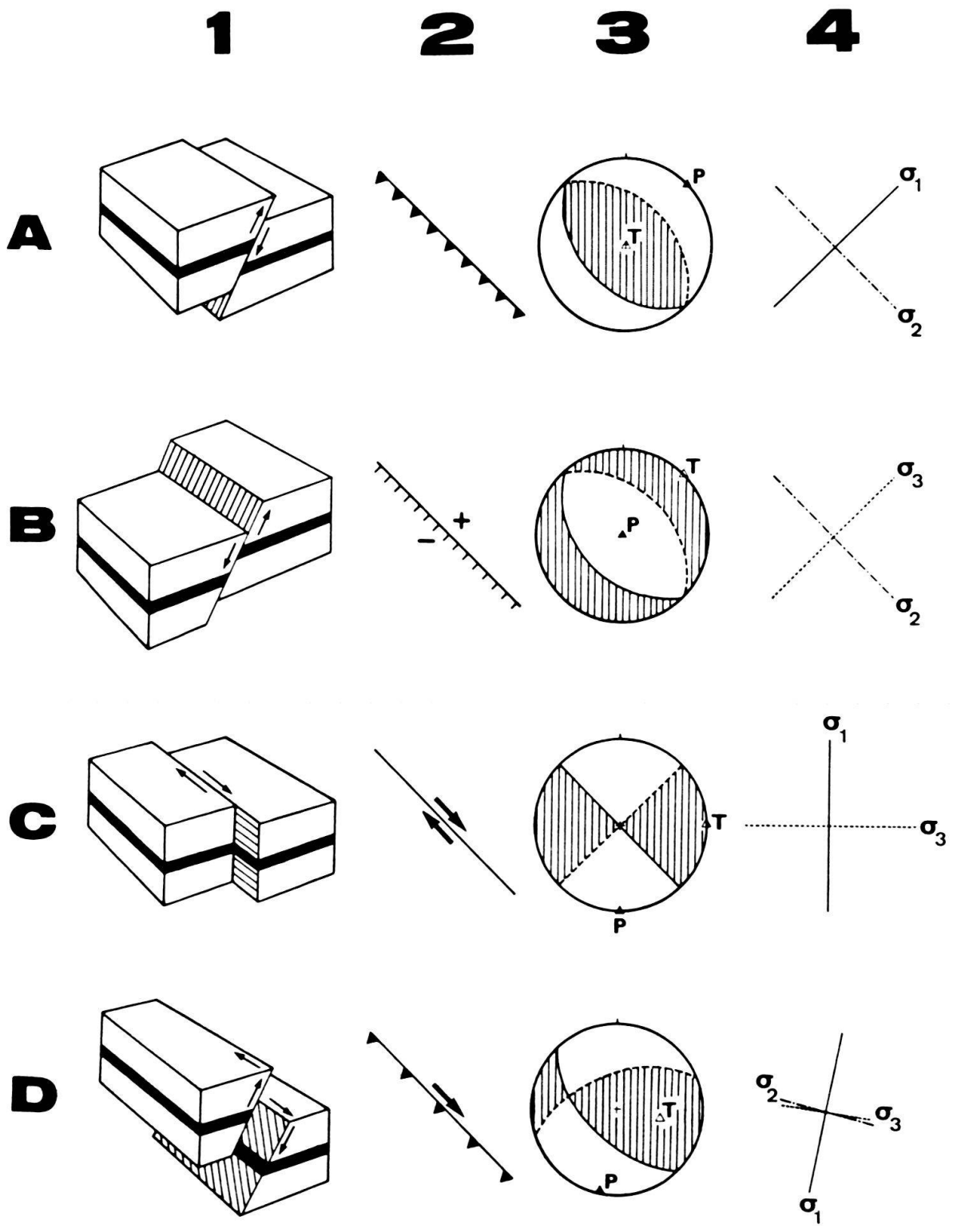

Fig. 4. Types of faulting, fault-plane solutions and principal stresses. *1*: Block diagram, *2*: Representation in the geological map, *3*: Fault-plane solution. *P*-wave radiation pattern and distribution of dilatational and compressional (hatched) quadrants. Lower hemisphere, equal area projection. *T*: *T*-axis, *P*: *P*-axis. Solid line: Fault plane. Dashed line: Auxiliary plane. *4*: Axes of principal stress projected into horizontal plane.

A: Reverse faulting, *B*: Normal faulting, *C*: Dextral strike-slip faulting, *D*: Oblique faulting.

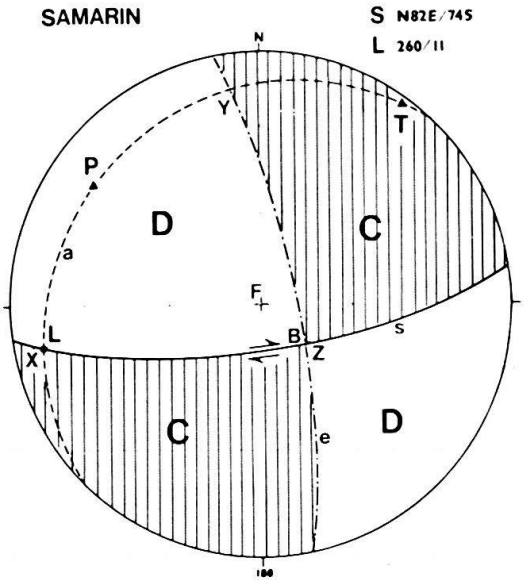

Fig. 5. Fault diagram, lower hemisphere, equal area projection. Locality: Six du Samarin, road near point 1592. Ultra-Helvetic Upper Jurassic limestone. Fault plane: Strike N82°E, dip 74°S. Slickensides: Trend N260°E, plunge 11°. Dash-point line: Trace of plane *E*. *P*: Axis of maximum shortening 306/20 (trend/plunge). *T*: Axis of maximum lengthening 36/03. Hatched: *C*-quadrants. Other notations see text, chapter 4.

5. Faulting in the Wildhorn seismic zone

For two selected sites within and near the Wildhorn zone observations of faulting are represented with the above method in Figures 5 and 6. The site represented in Figure 5 is located at Six du Samarin on the road St-Romain–Lac Zeuzier at about 1600 m altitude. Well exposed fault planes in upper Jurassic limestone striking N82°E and dipping 74°S show distinct, nearly horizontal slickensides (*L*: 260/11) demonstrating a dextral horizontal displacement along the fault planes. The axis of maximum shortening, indicated by *P* in Figure 5, plunges at 20° towards N306°E, the axis of maximum lengthening (*T* in Fig. 5) plunges at 3° towards N36°E.

Faulting in the massive, Upper Jurassic limestones of the Wildhorn nappe is beautifully exposed along the Sanetsch-Pass road in the Forêt des Rives region between Pont du Diable and Coppet. Figure 6 represents well-defined sinistral strike-slip faulting (*a*) and dextral strike-slip faulting (*b*) observed along the road cut at 1030 m altitude. The axis of maximum shortening *P* is nearly horizontal and shows a NW–SE orientation: 309/23 in Figure 6*a* and 133/08 in Figure 6*b*. The axis of maximum elongation *T* shows at NE–SW orientation: 216/09 in Figure 6*a* and 41/08 in Figure 6*b*.

The state of deformation corresponds very closely to the one observed 10 km to the northeast at Six du Samarin (Fig. 5). Similar, late-Alpine deformation along N–S sinistral and E–W dextral strike-slip faults is reported from the western Aar massif by Steck (1968). Within the crystalline rocks and the Mesozoic wedges of the central Aar massif and its northern border zone Labhart (1966) reports that the youngest Alpine movements occur along N–S striking vertical faults and produce oblique left-lateral displacements, with slickenside striations dipping 20–45° to the north.

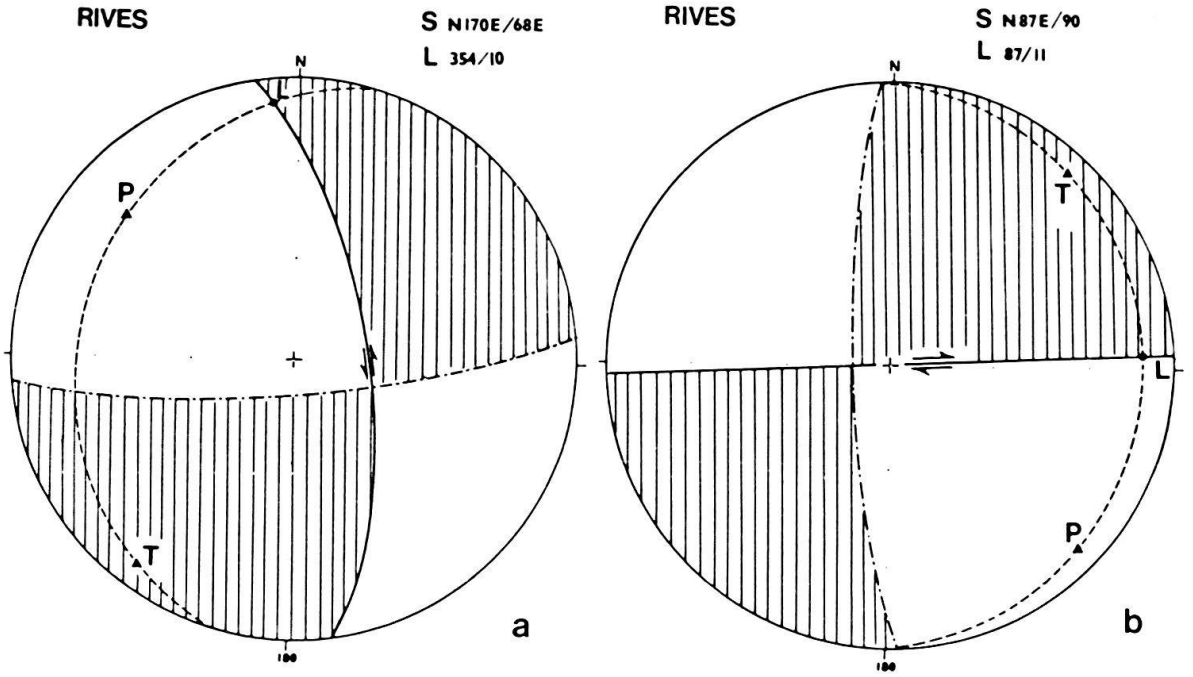

Fig. 6. Fault diagrams, lower hemisphere, equal area projection. Locality: Forêt des Rives, Sanetsch-Pass road, 1030 m elevation. Upper Jurassic limestone of the Wildhorn nappe. *a*) Sinistral strike-slip fault (solid trace line), strike N170°E, dip 68°E. Slickensides: Trend N354°E, plunge 10°. *P*: Axis of maximum shortening 309/23 (trend/plunge). *T*: Axis of maximum lengthening 216/09. Hatched: *C*-quadrants. *b*) Dextral, vertical strike-slip fault (solid trace line), strike N87°E. *L*: Slickensides, trend N87°E, plunge 11°. Dash-point line: Auxiliary plane. Hatched: *C*-quadrant. *P*: Axis of maximum shortening 133/08. *T*: Axis of maximum lengthening 41/08.

6. Discussion and comparison of seismological and geological data

The fault-plane solutions of strike-slip type shown in Figures 2 and 3 represent the predominant and characteristic types of focal mechanisms of the Wildhorn zone. But they are not the only ones to occur. Other types of fault-plane solutions, e.g. normal faulting on NW–SE striking fault planes, also have been observed.

The seismologically observed stress field of the Helvetic zone and upper crust of the Central Valais north of the Rhone river is characterized by NW–SE orientation of maximum compressive stress (*P*-axes) and NE–SW orientation of minimum compressive stress (*T*-axes). Fault-plane solutions of strike-slip type with dextral lateral displacement along E–W striking, steeply dipping nodal planes, and sinistral lateral displacement along N–S striking steeply inclined nodal planes, are predominant. A comparison of seismological (Fig. 2, 3) and structural data (Fig. 5, 6), facilitated by the analysis described in chapter 4, reveals the close relationship between the present tectonic movements and observed late-Alpine faulting. Obviously, the present stress field which causes the seismic activity of the Wildhorn zone appears to be very similar in its orientation to the stress field 5–15 million years ago which generated the neotectonic deformation of the Helvetic zone of the Central Valais.

Acknowledgments

I thank my colleagues of the Institute of Geophysics, Robert Berger, Hanspeter Boller, Markus Grieder and Dieter Mayer-Rosa for their great aid in the field operations and for many valuable discussions, William Lowrie and Roy Kligfield for critically reading the manuscript. Julien Fréchet, Grenoble, helped with reading seismograms of 1977 microearthquakes. Part of this work was supported by the Swiss National Science Foundation under Projects No. 2.658.72 and 2.202-0.74.

REFERENCES

BADOUX, H., BONNARD, E.G., BURRI, M., & VISCHER, A. (1959): *Atlas géologique de la Suisse 1:25000, Feuille n° 35, St-Léonard (avec notice explicative).* - Comm. géol. Suisse.

LABHART, T.P. (1966): *Mehrphasige alpine Tektonik am Nordrand des Aarmassivs.* - Eclogae geol. Helv. *59*/2, 803-830.

PAVONI, N. (1977): *An investigation of microearthquake activity in the Central Valais (Swiss Alps).* - Publ. Inst. Geophys. Pol. Acad. Sci. *116*, 317-320.

— (1980): *Crustal stresses inferred from fault-plane solutions of earthquakes and neotectonic deformation in Switzerland.* - Rock Mech. (Eng. Geol.) (in press).

STECK, A. (1968): *Die alpidischen Strukturen in den Zentralen Aaregraniten des westlichen Aarmassivs.* - Eclogae geol. Helv. *61*/1, 19-48.